https://doi.org/10.33261/jaaru.2025.32.4.004 *Association of Arab Universities Journal of Engineering Sciences (2025) 32(4):35-52*

Association of Arab Universities Journal of Engineering Sciences
مجلة اتحاد الجامعات العربية للدراسات والبحوث الهندسية

High-Resolution Direction Finding Exploiting the Additional Spatial Phase Shift Generated in Switched Parasitic Antenna Arrays.

Rabah Abduljabbar Jasem

AL-Dour Technical Institute, Northern Technical University, Salahudin, Iraq.

**Corresponding author:* Rabah Abduljabbar Jasem rabah_alobaidi5@yahoo.com rabah.aj@ntu.edu.iq

Published online: 31 December 2025

Abstract— The benefit of producing an additional spatial phase shift to signals received by a Switched Active Switched Parasitic Antenna (SASPA) array will be examined in this work. The additional spatial phase shift, along with the spatial phase shifts a received signal experiences while moving across an antenna array, greatly enhances the resolution of Direction of Arrival (DoA) estimation. It inherently occurs when each antenna in an SASPA array is switched from a parasitic to an active state while keeping the others as parasites at one time. The improvement is due to scaling the steering matrix of the measurements of a receiving SASPA array by a unitary matrix. The impact of this matrix resembles receiving the incoming signals with a greater Signal-to-Noise Ratio (SNR). Several simulations in this study depict that SASPA arrays can estimate the DoAs with a resolution much higher than that of all-active antenna arrays even when the array size is limited and the signals are received from critical directions and spatially very close to each other. The Root Mean Square Error (RMSE) criterion is examined as well, revealing that the estimated DoA using SASPA arrays closely matches the true value over a wide range of SNR.

Keywords— Direction of Arrival (DoA), MUSIC algorithm, SASPA arrays, RMSE criterion**.**

1. Introduction

Switched Parasitic Antenna (SPA) arrays provide several useful characteristics that are important for recent wireless communications. Among the features offered by these arrays are directivity, switched and steered radiation patterns, decreased interference, compact size, minimal hardware, and increased bandwidth [1, 6, 8, 13, 18, 21]. In [27], it is demonstrated that Circular Switched Parasitic Antenna (CSPA) array signifies affordable solution for small-cell mobile communications, where compact antennas with a flat steerable beam and an omnidirectional horizontal field of view are essential. In [26], a two active elements CSPA is proposed for WiMAX applications. A very early work on the use of parasitic antennas and their advantages in directing the radiation pattern of an omnidirectional antenna to a specific direction was the invention of the Yagi-Uda antenna in 1926. The array consists of several wire antenna elements with only one element acting as an active antenna, while the remaining elements act as parasites. The active element is powered by the RF signal when the array is in transmitting mode, while it is connected to the load when the array is in receiving mode. The parasitic elements have terminals that are short-circuited. Since their physical lengths are not tuned to the operating frequency, the parasites in Yagi-Uda antenna accumulate the power radiated from or received by the active element into one major main lobe with small side lobes. The result is a radiation pattern with a high gain and a very small beamwidth in one direction. However, this antenna array must be rotated mechanically to change the direction of its directive main lobe.

After the invention of PIN diodes, the state of each antenna element in an array can be changed very quickly and in a very short time. These diodes can be used as RF switches due to their fast switching, thus providing switched routes for RF frequencies to the antenna elements in antenna arrays. If an array consists of one element operating in an active state while the states of the other elements, which are parasites, can be changed between the states ON and OFF by employing PIN diodes, an SPA array can be constructed. In addition to the role of the active element, the number of parasitic

elements that are in the ON state in an SPA array plays a significant role in shaping the radiation pattern emitted by the array. Thus, SPA arrays possess an inherent ability to produce switched beams [6]. In addition to the scheme of changing the states of the parasites in an SPA array, the energy coupled from the active element to the parasites and vice versa plays another important role in shaping the resultant radiation pattern of an SPA array and its direction. Thus, SPA arrays are considered as one type of smart antenna array [6, 18, 31]. Several studies have been conducted on the performance of SPA arrays as transmitting antenna arrays, their capability of beamforming the radiation pattern, and their improvements in the transmission characteristics of antenna arrays, such as in [1, 6, 8, 13-16, 18, 30-32, 34] and others. Additionally, the contribution of SPA arrays in enhancing MIMO arrays has been discussed in [20, 22]. However, only few investigations have focused on the performance of SPA arrays as receiving arrays, and specifically, as direction- finding arrays as in [20, 23, 28].

If one element in an *N*-element SPA array is switched to an active state at one time while keeping the other elements in parasitic states, then this procedure is repeated sequentially for each element in the array; a Switched Active Switched Parasitic Antenna array (SASPA) can be obtained [6]. As a result, *N* distinct radiation patterns can be produced, each directed in a different direction. If the SASPA array's geometry is a Uniform Circular Array (UCA), then *N* symmetrical radiation patterns can be achieved. In addition to being beneficial as transmitting arrays, SASPA can be used for DoA estimation when used as receiving arrays, provided the element switching from an active to a parasitic state or vice versa occurs very rapidly within one measurement snapshot. Such an action is possible with PIN diodes.

The usefulness of SASPA as direction-finding arrays will be investigated in this work in conjunction with the well-known direction-finding algorithm, Multiple Signal Classification (MUSIC). When signals impinge on an SASPA array, the energy that is energized in each element due to these signals will be mutually coupled from the parasites to the active element, and vice versa. The exchange of this induced energy and the sequential switching of each element in an SASPA array to the active state help to improve the resolution of the DoA estimate. This occurs because a unitary matrix, which scales the steering matrix of SASPA arrays, can be generated from the measurements of these arrays. The elements of this matrix are a function of the additional spatial phase shift a signal undergoes during the transition of a parasitic element in the array to the active state, in addition with the typical spatial phase shift caused by the propagation delay of the received signal throughout the array.

2. Data Model of a Receiving SASPA Array

Let an SASPA array consist of *N* identical antenna elements, such as half-wave dipole antennas with *d* inter-element spacing. Fig.1 shows an SASPA with structures as a Uniform Linear Array (ULA-SASPA) and a Uniform Circular Array (UCA-SASPA), respectively. The array is receiving *M* narrowband signals. The signals received by the array are supposed to be incident in the *x-y* plane. Fig.2 illustrates how the energy, which is energized by the received signal in the elements of the SASPA array, is accumulated at the active element via the mutual coupling phenomenon during one sub-snapshot. The measurement obtained from the load of the active element reflects the effect of the received signal in this element, as well as the effect of the retransmitted energies from the parasites and received by the active element through the mutual coupling. Thus, within a single measurement snapshot, there will be *N* frames of measurements with each frame consisting of *N* sub-measurements, i.e., N^2 measurements. Each sub-measurement frame is carried out when a certain element in the SASPA array is active. It is assumed that the time required to implement *N* sub-measurements during one snapshot measurement is very short, and it is considered almost instantaneous. This means that the phase shift caused by the time transition from one sub-measurement to another within a single snapshot can be ignored. This is feasible with very high-speed PIN diodes and narrowband received signals. For one signal with a strength $\mathrm{v}(t)$ received by the array from the azimuth direction ϕ, the nondirectional sub-measurement when element *n* is active will be:

$$\mathbf{y}^{(n)}(t) = \mathbf{C}^{(n)}\mathbf{u}\,(\phi)\mathrm{v}(t) \tag{1}$$

with

$$\mathbf{y}^{(n)}(t) = [0 \;\; 0 \;\; \mathrm{y}_n(t) \;\; 0 \;\; \cdots 0]^T \in \mathbb{C}^{N\times 1} \tag{2}$$

The matrix $\mathbf{C} \in \mathbb{C}^{N\times N}$ is the mutual coupling matrix**.** The common structure of $\mathbf{C}$ is:

$$\mathbf{C} = \begin{bmatrix} c_{11} & c_{12} & c_{13} & \cdots & c_{1N} \\ c_{21} & c_{22} & c_{23} & \cdots & c_{2N} \\ c_{31} & c_{32} & c_{33} & \cdots & c_{3N} \\ \vdots & \vdots & \vdots & \ddots & \vdots \\ c_{N1} & c_{N2} & c_{N3} & \cdots & c_{NN} \end{bmatrix} \tag{3}$$

In the case of the ULA array, $\mathbf{C}$ has a Toeplitz structure, while it has a Circulant Toeplitz structure when the array is UCA. In [24], a novel mutual coupling model, Coupled Voltages to Uncoupled Currents (CVUC), is derived as a general model for a receiving antenna array. It is also verified in [24] that the CVUC model applies to SASPA arrays after setting $Z_L = 0$ for the parasitic elements. When element #1 is active, the measurement (1) and the matrix $\mathbf{C}$ will be, respectively:

$$\mathbf{y}^{(1)}(t) = \mathbf{C}^{(1)}\mathbf{u}\,(\phi)\mathrm{v}(t) \tag{4}$$

$$\mathbf{C}^{(1)} = \begin{bmatrix} c_{11} & c_{12} & c_{13} & \cdots & c_{1N} \\ 0 & 0 & 0 & \cdots & 0 \\ 0 & 0 & 0 & \cdots & 0 \\ \vdots & \vdots & \vdots & \ddots & \vdots \\ 0 & 0 & 0 & \cdots & 0 \end{bmatrix} \tag{5}$$

The vector, $\mathbf{u}(\phi)$, which is known as the steering vector, represents the response of the array to the incoming signal. Each entry of this vector is the gain of the element multiplied by the spatial phase shift resulting from the propagation delay caused by moving the received signal from element to element. Assuming the gain of each element is unity due to the half-wave dipole antenna assumption, $\mathbf{u}(\phi)$ in the case of the ULA array is defined as:

$$\mathbf{u}_{ULA}(\phi) = [1 \quad e^{jkd\cos\phi} \quad \dots \quad e^{j(N-1)kd\cos} \quad]^T \in \mathbb{C}^{N\times 1} \qquad (6)$$

For a UCA array with a radius R, $\mathbf{u}(\phi)$ is defined as:

$$\mathbf{u}_{UCA}(\phi) = \left[e^{jkR\cos\phi} \quad e^{jkR\cos\left(\phi-2\pi\frac{1}{N}\right)} \quad \dots \quad e^{jkR\cos\left(\phi-2\pi\frac{N-1}{N}\right)}\right]^T \in \mathbb{C}^{N\times 1} \quad \dots . \quad (7)$$

Thus, (6) and (7) contain only the progressive spatial shifts a received signal undergoes due to the propagation delays when this signal moves across the array.

Among the aforementioned characteristics of the SASPA array is its self-beamforming capability. This means that the analysis with SASPA arrays should be conducted in beam space rather than in element space. Thus, the measurement obtained from an SASPA array within one sub-snapshot reflects the response of the directive beam of the overall radiation pattern an SASPA array produces when a certain element in the array is active. Therefore, a single value, developed across the terminals of the load of the active element, will be assigned to that sub-snapshot. This single-valued measurement is the active element's response to the incident signal as well as the coupled responses of the parasites into the active element via the mutual coupling phenomenon. Consequently, equation (1) should be pre-multiplied by $\mathbf{u}^H(\phi)$ [10, 35], where $(.^H)$ denotes the Hermitian operation, to obtain directivity and to be in the beam space. Accordingly, the measurement at the terminals of the active element n will be:

$$\mathrm{z}^{(n)}(t) = \mathbf{u}^H(\phi)\mathbf{y}^{(n)}(t) = \mathbf{u}^H(\phi)\mathbf{C}^{(n)}\mathbf{u}(\phi)\mathrm{v}(t) \dots . \quad (8)$$

Thus, $\mathrm{z}^{(n)}(t)$ for the ULA-SASPA and UCA-SASPA arrays will be, respectively:

$$\mathrm{z}^{(n)}_{ULA-SASPA}(t) = e^{-j(n-1)kd\cos\phi}\mathbf{c}^{(n)^T}\mathbf{u}_{ULA}(\phi)\mathrm{v}(t) \quad (9)$$

$$\mathrm{z}^{(n)}_{UCA-SASP}(t) = e^{-jkR\cos\left(\phi-2\pi\frac{n-1}{N}\right)}\mathbf{c}^{(n)^T}\mathbf{u}_{UCA}(\phi)\mathrm{v}(t) \quad \dots . \quad (10)$$

Where $\mathbf{c}^{(n)^T}$ is row n of the coupling matrix $\mathbf{C}^{(n)}$ and T is the transpose operation. Note that equations (9) and (10) indicate that making one element active while keeping the other elements in parasitic states in an SASPA array adds a spatial phase shift to the received signal in addition to its propagation delays as it moves across the array. Fig.2 shows how the additional phase shift occurs. When M signals coming from azimuth directions $\phi_m \; m = 1, 2, \cdots M$ are received by the array, (9) becomes:

$$\mathrm{z}^{(n)}_{ULA-SASPA}(t) = e^{-j(n-1)kd\,co\quad{}_1}\mathbf{c}^{(n)^T}\mathbf{u}_{ULA}(\phi_1)\mathrm{v}_1(t) + e^{-j(n-1)kd\cos\phi_2}\mathbf{c}^{(n)^T}\mathbf{u}_{ULA}(\phi_2)\mathrm{v}_2(t) + \cdots + e^{-j(n-1)kd\cos\phi_M}\mathbf{c}^{(n)^T}\mathbf{u}_{ULA}(\phi_M)\mathrm{v}_M(t) \quad \dots . \quad (11)$$

Or

$$\mathrm{z}^{(n)}_{ULA-SASPA}(t) = \mathbf{c}^{(n)^T}\mathbf{U}_{ULA}\mathbf{\Theta}^{n-1}\mathbf{v}(t) \qquad (12)$$

Where $\mathbf{U}_{ULA}$ is the steering matrix of a ULA array and is defined as:

$$\mathbf{U}_{ULA}(\phi) = \begin{bmatrix} 1 & 1 & \cdots & 1 \\ e^{jkd\,co\quad{}_1} & e^{jkd\cos\phi_m} & \cdots & e^{jkd\cos\phi_M} \\ e^{j2kd\cos\phi_1} & e^{j2kd\cos\phi_m} & \cdots & e^{j2kd\cos\phi_M} \\ \vdots & \vdots & \ddots & \vdots \\ e^{j(N-1)kd\cos\phi_1} & e^{j(N-1)kd\cos\phi_m} & \cdots & e^{j(N-1)kd\cos\phi_M} \end{bmatrix} \quad \dots . \quad (13)$$

$$\mathbf{\Theta}^{n-1} = \mathrm{diag}\left(e^{-j(n-1)kd\cos\phi_1}, \; e^{-j(n-1)kd\,co\quad{}_2}, \; \dots, \; e^{-j(n-1)kd\,co\quad{}_M}\right) \qquad (14)$$

$$\mathbf{v}(t) = [\mathrm{v}_1(t) \quad \mathrm{v}_2(t) \quad \cdots \quad \mathrm{v}_M(t)]^T \qquad (15)$$

Following the same procedure, (10) becomes:

$$\mathrm{z}^{(n)}_{UCA-SASPA}(t) = \mathbf{c}^{(n)^T}\mathbf{U}_{UCA}\mathbf{\Psi}^{(n)}\mathbf{v}(t) \qquad (16)$$

With $\mathbf{U}_{UCA}$ as the steering matrix of a UCA array:

$$\mathbf{U}_{UCA}(\phi) = \begin{bmatrix} e^{jkR\cos\phi_1} & e^{jkRr\cos\phi_m} & e^{jkR\cos\phi_M} \\ e^{jkR\cos\left(\phi_1-\frac{2\pi}{N}\right)} & e^{jkRr\cos\left(\phi_m-\frac{2\pi}{N}\right)} & e^{jkR\cos\left(\phi_M-\frac{2\pi}{N}\right)} \\ e^{jkR\cos\left(\phi_1-\frac{4\pi}{N}\right)} & e^{jkR\cos\left(\phi_m-\frac{4\pi}{N}\right)} & e^{jkR\cos\left(\phi_M-\frac{4\pi}{N}\right)} \\ \vdots & \vdots & \vdots \\ e^{jkR\cos\left(\phi_1-\frac{2\pi(N-1)}{N}\right)} & e^{jkR\cos\left(\phi_m-\frac{2\pi(N-1)}{N}\right)} & e^{jkR\cos\left(\phi_M-\frac{2\pi(N-1)}{N}\right)} \end{bmatrix} \quad \dots . \quad (17)$$

$$\mathbf{\Psi}^{(n)} = \mathrm{diag}\left(e^{-jkR\cos\left(\phi_1-2\pi\frac{n-1}{N}\right)}, \; \dots, \; e^{-jkR\cos\left(\phi_M-2\pi\frac{n-1}{N}\right)}\right) \qquad (18)$$

Observe that the matrix $\mathbf{\Theta}^{n-1}$ in (14) is the matrix $\mathbf{\Theta}$ elevated to the exponent$(n-1)$, while $\mathbf{\Psi}^{(n)}$ in (18) denotes the matrix $\mathbf{\Psi}$ at index n. As mentioned above, the unitary matrices $\mathbf{\Theta}^{n-1}$ and $\mathbf{\Psi}^{(n)}$ depend on the additional phase shifts that occur to all received signals in an SASPA array. It now follows that, by gathering the N frames of sub-measurements taken within one snapshot, the noisy ULA-SASPA array output for that snapshot is:

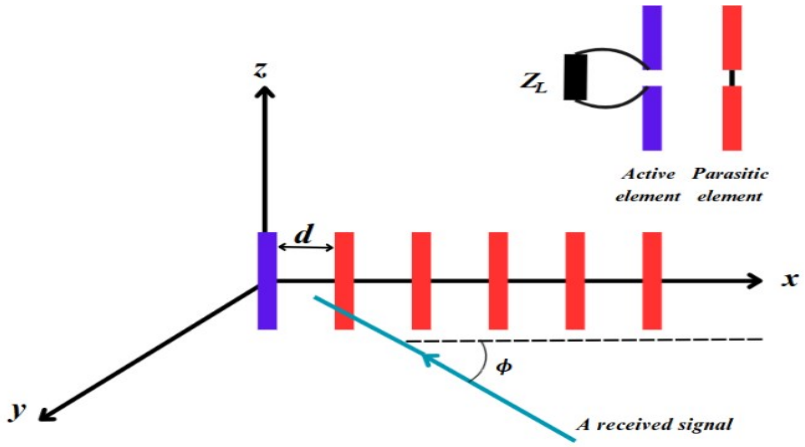

a) A ULA-SASPA array

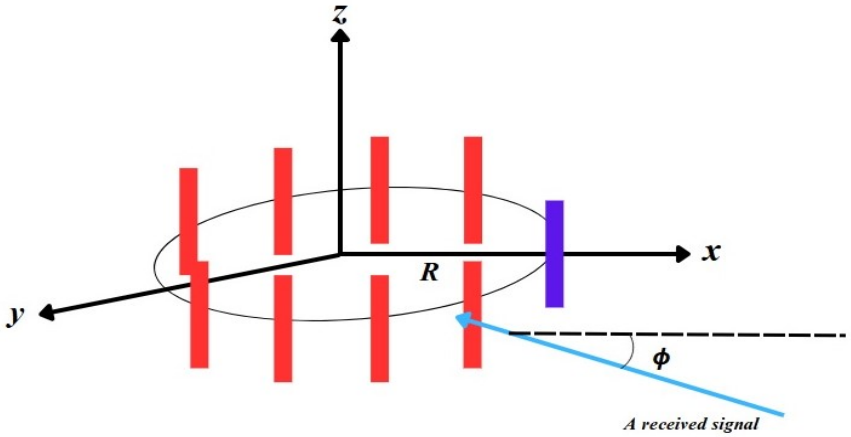

b) A UCA-SASPA array

Figure 1: Two geometries of the SASPA array.

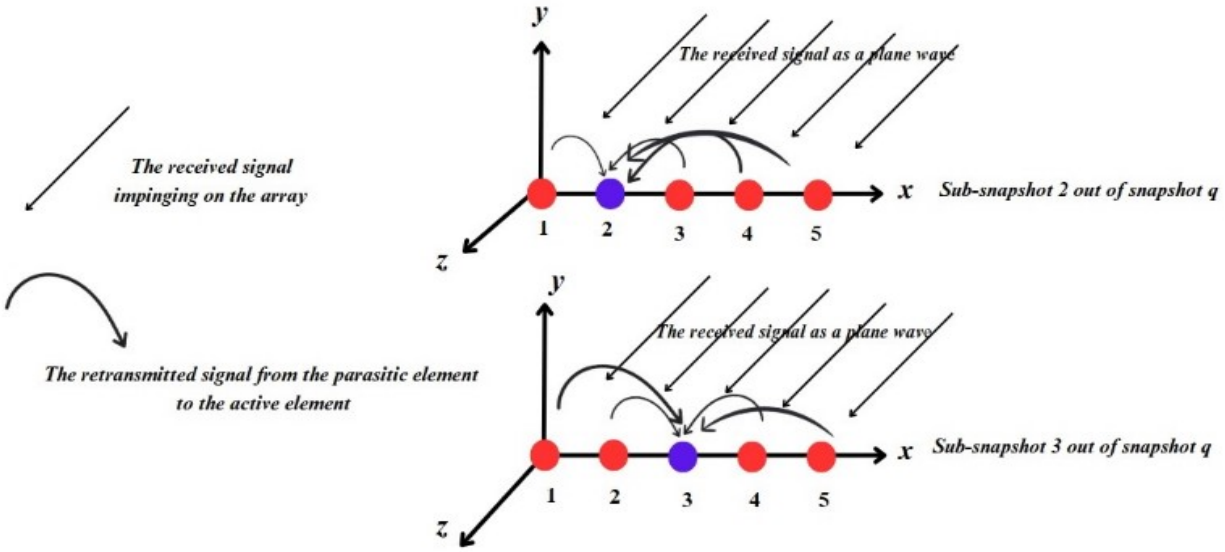

Figure 2: The performance of an SASPA array during two successive sub measurements.

$$\mathbf{z}_{ULA-SASPA}(t)=\begin{bmatrix} z^{(1)}_{ULA-SASPA}(t)\\ z^{(2)}_{ULA-SASPA}(t)\\ z^{(3)}_{ULA-SASPA}(t)\\ \vdots\\ z^{(N)}_{ULA-SASPA}(t)\end{bmatrix}=$$

$$\begin{bmatrix} \left(\mathbf{c}^{(1)}\right)^T\mathbf{U}_{ULA}\\ \left(\mathbf{c}^{(2)}\right)^T\mathbf{U}_{ULA}\boldsymbol{\Theta}\\ \left(\mathbf{c}^{(3)}\right)^T\mathbf{U}_{ULA}\boldsymbol{\Theta}^2\\ \vdots\\ \left(\mathbf{c}^{(N)}\right)^T\mathbf{U}_{ULA}\boldsymbol{\Theta}^{N-1}\end{bmatrix}\mathbf{v}(t)+\begin{bmatrix}\left(\mathbf{c}^{(1)}\right)^T\mathbf{n}^{(1)}(t)\\ \left(\mathbf{c}^{(2)}\right)^T\mathbf{n}^{(2)}(t)\\ \left(\mathbf{c}^{(3)}\right)^T\mathbf{n}^{(3)}(t)\\ \vdots\\ \left(\mathbf{c}^{(N)}\right)^T\mathbf{n}^{(N)}(t)\end{bmatrix}$$

(19)

Note that the vector $\mathbf{n}^{(n)}(t)$ in (19) is the noise vector when element *n* is active. This noise is assumed to be Additive White Gaussian Noise (AWGN) with zero mean and is uncorrelated with the received signals. The vector $\mathbf{n}^{(n)}(t)$ is defined as:

$$\mathbf{n}^{(n)}=\begin{bmatrix} n_1^{(n)} & n_2^{(n)} & \cdots & n_N^{(n)}\end{bmatrix}^T \tag{20}$$

Also, it is assumed that this noise exists in the surroundings or periphery of the array. This noise, therefore, is affected by the mutual coupling [29]. Thus, the complex value $\left(\mathbf{c}^{(n)}\right)^T\mathbf{n}^{(n)}(t)$ represents the coupled noise at element *n*. The system (19) can be rewritten as:

$$\mathbf{z}_{ULA-SASPA}(t)=$$
$$\begin{bmatrix} \left(\mathbf{c}^{(1)}\right)^T & \cdots & \mathbf{0} & \mathbf{0}\\ \mathbf{0} & \ddots & \mathbf{0} & \mathbf{0}\\ \vdots & & \vdots & \vdots\\ \mathbf{0} & \cdots & \mathbf{0} & \left(\mathbf{c}^{(N)}\right)^T\end{bmatrix}\begin{bmatrix}\mathbf{U}_{ULA}\mathbf{v}(t)+\mathbf{n}^{(1)}(t)\\ \mathbf{U}_{ULA}\boldsymbol{\Theta}\mathbf{v}(t)+\mathbf{n}^{(2)}(t)\\ \mathbf{U}_{ULA}\boldsymbol{\Theta}^2\mathbf{v}(t)+\mathbf{n}^{(3)}(t)\\ \vdots\\ \mathbf{U}_{ULA}\boldsymbol{\Theta}^{N-1}\mathbf{v}(t)+\mathbf{n}^{(N)}(t)\end{bmatrix}=$$
$$\bar{\mathbf{C}}\begin{bmatrix}\mathbf{U}_{ULA}\mathbf{v}(t)+\mathbf{n}^{(1)}(t)\\ \mathbf{U}_{ULA}\boldsymbol{\Theta}\mathbf{v}(t)+\mathbf{n}^{(2)}(t)\\ \mathbf{U}_{ULA}\boldsymbol{\Theta}^2\mathbf{v}(t)+\mathbf{n}^{(3)}(t)\\ \vdots\\ \mathbf{U}_{ULA}\boldsymbol{\Theta}^{N-1}\mathbf{v}(t)+\mathbf{n}^{(N)}(t)\end{bmatrix}=\bar{\mathbf{C}}\mathbf{A}(t)$$

(21)

Where each zero entry in the matrix $\bar{\mathbf{C}}\in\mathbb{C}^{N\times N^2}$ in (21) is a vector with zero entries and size $1\times N$. The vector $\mathbf{A}(t)\in\mathbb{C}^{N^2\times 1}$ denotes the measurements that are free from the mutual coupling effect. The system (21) is underdetermined because it comprises *N* equations in N^2 unknowns. The Least Squares (LS) technique can be applied to find the minimum solution for this type of system, which is:

$$\mathbf{A}(t)=\bar{\mathbf{C}}^H(\bar{\mathbf{C}}\bar{\mathbf{C}}^H)^{-1}\mathbf{z}_{ULA-SASP}\ (t) \tag{22}$$

Observe that $\bar{\mathbf{C}}$ possesses full row rank, meaning $\text{rank}(\bar{\mathbf{C}})=N$. Assuming that $\bar{\mathbf{C}}$ is known, the vector $\mathbf{A}(t)$ can be rewritten as:

$$\mathbf{A}(t)=\begin{bmatrix}\mathbf{A}^{(1)}(t)\\ \mathbf{A}^{(2)}(t)\\ \vdots\\ \mathbf{A}^{(N)}(t)\end{bmatrix}=\begin{bmatrix}\mathbf{U}_{ULA}\mathbf{v}(t)+\mathbf{n}^{(1)}(t)\\ \mathbf{U}_{ULA}\boldsymbol{\Theta}\mathbf{v}(t)+\mathbf{n}^{(2)}(t)\\ \vdots\\ \mathbf{U}_{ULA}\boldsymbol{\Theta}^{N-1}\mathbf{v}(t)+\mathbf{n}^{(N)}(t)\end{bmatrix}$$

(23)

Where $\mathbf{A}^{(n)}(t)$ is the measurement vector when element *n* is active after counteracting the mutual coupling effect. Summing up these *N* measurements' yields:

$$\boldsymbol{\gamma}(t)=\sum_{n=1}^{N}\mathbf{A}^{(n)}(t)=\mathbf{U}_{ULA}(\sum_{n=1}^{N}\boldsymbol{\Theta}^{n-1})\mathbf{v}(t)+\sum_{n=1}^{N}\mathbf{n}^{(n)}(t)$$

(24)

The covariance matrix, $\mathbf{R}_{ULA-SASPA}\in\mathbb{C}^{N\times N}$ of the measurements in (24) is then:

$$\mathbf{R}_{ULA-SASPA}=E\left(\boldsymbol{\gamma}(t)\boldsymbol{\gamma}^H(t)\right)$$
$$=$$
$$E\left[\left\{\mathbf{U}_{ULA}(\sum_{n=1}^{N}\boldsymbol{\Theta}^{n-1})\mathbf{v}(t)+\sum_{n=1}^{N}\mathbf{n}^{(n)}(t)\right\}\left\{\mathbf{U}_{ULA}(\sum_{n=1}^{N}\boldsymbol{\Theta}^{n-1})\mathbf{v}(t)+\sum_{n=1}^{N}\mathbf{n}^{(n)}(t)\right\}^H\right]=$$
$$\mathbf{U}_{ULA}(\sum_{n=1}^{N}\boldsymbol{\Theta}^{n-1})E\left(\mathbf{v}(t)\mathbf{v}^H(t)\right)(\sum_{n=1}^{N}\boldsymbol{\Theta}^{n-1})^H\mathbf{U}_{ULA}^H+$$
$$E\left(\mathbf{n}(t)\mathbf{n}^H(t)\right)=\mathbf{U}_{ULA}\mathbf{G}\mathbf{V}\mathbf{G}^{\boldsymbol{H}}\mathbf{U}_{ULA}^H+\sigma^2\mathbf{I}_N \tag{25}$$

With

$$\mathbf{V}=E[\mathbf{v}(t)\mathbf{v}(t)^H]\in\mathbb{C}^{M\times M} \tag{26}$$

$$\mathbf{G}=\sum_{n=1}^{N}\boldsymbol{\Theta}^{n-1}\in\mathbb{C}^{M\times M} \tag{27}$$

$$\mathbf{n}(t)=\sum_{n=1}^{N}\mathbf{n}^{(n)}(t)\in\mathbb{C}^{N\times 1} \tag{28}$$

The covariance of the noise $\mathbf{n}(t)$ is:

$$E[\mathbf{n}(t)\mathbf{n}(t)^H]=\begin{bmatrix}\sigma_1^2 & 0 & \ldots & 0\\ 0 & \sigma_2^2 & & 0\\ \vdots & & \ddots & \vdots\\ 0 & 0 & \ldots & \sigma_N^2\end{bmatrix}\approx\sigma^2\mathbf{I}_N \tag{29}$$

Where $\mathbf{I}_N$ is the *N*-by-*N* identity matrix. The same procedure that was used to derive the equations (19)-(25) can be applied to further process the $z^{(n)}_{UCA-SASPA}(t)$ in (16) to obtain:

$$\mathbf{R}_{UCA-SASPA}=\mathbf{U}_{UCA}\,\mathbf{X}\mathbf{V}\mathbf{X}^{\boldsymbol{H}}\mathbf{U}_{UCA}^H+\sigma^2\mathbf{I}_N \tag{30}$$

$$\mathbf{X}=\sum_{n=1}^{N}\boldsymbol{\Psi}^{(n)}\in\mathbb{C}^{M\times M}$$

(31)

3. Scaling The Steering Matrix in The SASPA Array

Eigen decomposing the covariance matrices $\mathbf{R}_{ULA-SASPA}$ and $\mathbf{R}_{UCA-SASPA}$ results in calculating the corresponding signal and noise subspaces. The relationship between the steering matrix and the signal subspace, which is obtained from the measurements of the SASPA array, can be defined as [11, 25, 33]:

$$\mathbf{E}_{s,ULA-SASPA} = \mathbf{U}_{ULA}\left(\sum_{n=1}^{N}\mathbf{\Theta}^{n-1}\right)\mathbf{T}_{ULA-SASPA} = \mathbf{U}_{ULA}\mathbf{G}\mathbf{T}_{ULA-SASPA} \quad (32)$$

$$\mathbf{E}_{s,UCA-SASPA} = \mathbf{U}_{UCA}\left(\sum_{n=1}^{N}\mathbf{\Psi}^{(n)}\right)\mathbf{T}_{UCA-SASPA} = \mathbf{U}_{UCA}\mathbf{X}\mathbf{T}_{UCA-SASPA} \quad (33)$$

where $\mathbf{T}_{ULA-SASPA} \in \mathbb{C}^{M\times M}$ and $\mathbf{T}_{UCA-SASPA} \in \mathbb{C}^{M\times M}$ are invertible matrices that rotate the matrices $\mathbf{U}_{ULA}\mathbf{G}$ and $\mathbf{U}_{UCA}\mathbf{X}$ into their associated signal subspaces $\mathbf{E}_{s,ULA-SASPA}$ and $\mathbf{E}_{s,UCA-SASPA}$, respectively. Also, note that, $\mathbf{G}$ and $\mathbf{X}$ are diagonal and positive definite matrices.

Thus, both matrices $\mathbf{G}$ and $\mathbf{X}$ have row-scaled the corresponding rotation matrices $\mathbf{T}_{ULA-SASPA}$ and $\mathbf{T}_{UCA-SASPA}$, as indicated by (32) and (33). The matrix $\mathbf{G}$ can be approximated to $N\mathbf{I}_N$ (see section 4.2) at the corresponding DoAs, if the inter-element spacing is set as a fraction of the wavelength of the received signal, λ, (to be determined later), along with certain limitations on the directions of these signals. Similarly, if the radius of a UCA-SASPA array is a fraction of λ, the matrix $\mathbf{X}$ can be approximated to $NJ_0(kR)\mathbf{I}_N$, where $J_0(\cdot)$ denotes the Bessel function of the first kind of order zero. This holds true regardless of the directions of the incoming signals. The beneficial effect of these scaling matrices on the associated covariance matrices (25) and (30) concerning eigen decomposition can be clarified as follows.

Assume the array is receiving uncorrelated signals $\mathbf{v}(t) = [\mathrm{v}_1(t)\ \ \mathrm{v}_2(t)\ \ \cdots\ \ \mathrm{v}_M(t)]^T$, leading to the signal covariance matrix being diagonal, i.e., $\mathbf{V} = E[\mathbf{v}(t)\mathbf{v}^H(t)] = \mathrm{diag}(\propto_1^2, \dots, \propto_M^2)$ where $\propto_m^2$ represents the power of the mth received signal. Therefore, the entries of $\mathbf{V}$ are positive elements. Now, since $\mathbf{G}$ and $\mathbf{X}$ are also diagonal matrices, it follows that

$$\mathbf{G}\mathbf{V}\mathbf{G}^H = \mathbf{G}\mathbf{G}^H\mathbf{V} = \mathrm{diag}(|g_1|^2 \propto_1^2,\ \dots,\ |g_M|^2 \propto_M^2) \quad (34)$$

$$\mathbf{X}\mathbf{V}\mathbf{X}^H = \mathbf{X}\mathbf{X}^H\mathbf{V} = \mathrm{diag}(|x_1|^2 \propto_1^2,\ \dots,\ |x_M|^2 \propto_M^2) \quad (35)$$

where g_m and x_m are the mth diagonal elements of $\mathbf{G}$ and $\mathbf{X}$, respectively. Each element in $\mathbf{G}\mathbf{G}^H$ or $\mathbf{X}\mathbf{X}^H$ is greater than one, i.e., $|g_m|^2 > 1$ and $|x_m|^2 > 1$, as will be shown in the following sections. Thus, in comparison to an identical all-active antenna array having the same geometry, and receiving the same signals, the effect of the matrices $\mathbf{G}\mathbf{V}\mathbf{G}^H$ or $\mathbf{X}\mathbf{V}\mathbf{X}^H$ is similar to receiving the signals with a higher SNR. In [19], it is shown that increasing the SNR of the received signals can reduce the leakage from the signal subspace into the noise subspace. Furthermore, in [17], it is shown that the eigenvalues of the signal subspace are also enlarged by increasing the SNR. As a result, more precise DoA estimation will be achieved when utilizing $\hat{\mathbf{E}}_{s,ULA-SASPA}$ or $\hat{\mathbf{E}}_{s,UCA-SASPA}$ within DoA algorithms such as MUSIC.

4. DoA Estimation with an SASPA Array.

In the following sections, the advantages of SASPA as direction finding arrays will be illustrated through their enhancement of the performance of the well-known DoA algorithm, MUSIC. The cost function of this algorithm is:

$$P_{MUSIC}(\phi) = \frac{1}{\mathbf{u}^H(\phi)\hat{\mathbf{E}}_n\hat{\mathbf{E}}_n^H\mathbf{u}(\phi)} = \frac{1}{\|\hat{\mathbf{E}}_n^H\mathbf{u}(\phi)\|^2} = \frac{1}{\mathbf{u}^H(\phi)(\mathbf{I}-\hat{\mathbf{E}}_S\hat{\mathbf{E}}_S^H)\,\mathbf{u}(\phi)} \quad (36)$$

In (36), $\hat{\mathbf{E}}_n \in \mathbb{C}^{N\times(N-M)}$, and $\hat{\mathbf{E}}_s \in \mathbb{C}^{N\times M}$ are the estimated noise and signal subspaces, respectively, calculated from the eigen decomposition of the covariance matrix of the measurements obtained from a receiving antenna array. $\mathbf{u}(\phi)$ is the search vector for the entire set $\{-\pi, \pi\}$ and is defined as in (6) or (7). The cost function (36) exhibits peaks at ϕ_s where s is a subset of the set$\{-\pi, \pi\}$, at which the corresponding $\mathbf{u}(\phi_s)$ is orthogonal to $\hat{\mathbf{E}}_n$.

Another criterion that measures the capability of SASPA arrays in improving the DoA estimation is by investigating the Root Mean Square Error (RMSE). This measure is calculated using:

$$RMSE = \sqrt{\frac{\sum_{i=1}^{L}(\hat{\phi}_i-\phi_i)^2}{L}} \quad (37)$$

$\hat{\phi}_i$ and ϕ_i are the estimated and actual DoA, respectively. L is the number of runs.

4.1 ULA-SASPA Array.

Recall $\mathbf{G}$ in (27). Every element in the diagonal matrix $\mathbf{\Theta}^{n-1}$ takes the form $e^{-j(n-1)kd\cos\phi_m}$, $m = 1,2,\dots,M$. Summing the N such terms give (see the next section):

$$\mathbf{G} = \mathrm{diag}\left(\frac{sin\left(\frac{N\psi_1}{2}\right)}{sin\left(\frac{\psi_1}{2}\right)}e^{j\frac{(N-1)\psi_1}{2}},\ \dots,\ \frac{sin\left(\frac{N\psi_M}{2}\right)}{sin\left(\frac{\psi_M}{2}\right)}e^{j\frac{(N-1)\psi_M}{2}}\right) \quad (38)$$

Where,

$$\psi_m = kd\cos\phi_m \quad (39)$$

If the array is placed along the x-axis and symmetrically distributed around the y-axis, the phase shift term in (38) can be removed. The steering vector $\mathbf{u}_{ULA-SASPA}(\psi_m)$ is then:

$$\mathbf{u}_{ULA-SASPA}(\psi_m) = \left(\frac{sin\left(\frac{N\psi_m}{2}\right)}{sin\frac{\psi_m}{2}}\right)[1 \quad e^{j\psi_m} \quad \dots \quad e^{j(N-1)\psi_m}]^T$$

$$= f(\psi_m)\mathbf{u}_{ULA}(\psi_m) \quad (40)$$

In the case of a ULA-SASPA array, (36) should be updated to:

$$P_{MUSIC}(\phi) = \frac{1}{f(\psi_m)^*\mathbf{u}^H(\phi)\hat{\mathbf{E}}_{n,ULA-SASPA}\hat{\mathbf{E}}_{n,ULA-SASP}^H\ f(\psi_m)\mathbf{u}(\phi)}$$

$$= \frac{1}{\left\|\hat{\mathbf{E}}_{n,ULA-SASPA}^{H} f(\psi_m)\mathbf{u}(\phi)\right\|^2} \quad (41)$$

Observe that when of ψ_m takes very small values, $f(\psi_m)$ can be approximated to N, which means that the matrix $\mathbf{G}$ transforms to the matrix $N\mathbf{I}_N$ at the corresponding ϕ_m. Thus, the rows of the matrix $\mathbf{T}_{ULA-SASP}$ are scaled by a positive definite matrix. Consequently, a larger reduction in the distance metric between $\mathbf{U}_{ULA}$ and the estimated signal subspace $\hat{\mathbf{E}}_{s,ULA-SASPA}$ will be accomplished at the related ϕ_m.

All-active antenna arrays with only dipole elements estimate the DoA of received signals exploiting only the propagation delay of the received signal across the array, as the gain of each element is unity, i.e., $f(\psi_i) = 1$. In the case of SASPA arrays consisting omnidirectional antenna elements, other factors that inherently exist, gain and directivity, are provided by these arrays in addition to the propagation delay effect. These factors may enhance the accuracy of DoA estimation. In [3], it is demonstrated that enhanced DoA estimation can be achieved when every antenna element in the array is active and directional. Thus, omnidirectional-element ULA-SASPA arrays outperform omnidirectional-element all-active ULA arrays. This advantage is evident through the eigenvalues of the signal subspace of an array, which are greater when the array is a ULA-SASPA array in comparison to the all-active array with the same structure and the same number of omnidirectional antenna elements. Consequently, the possibility of some signal subspace merging with the noise subspace will be greatly diminished when ULA-SASPA arrays are used. The factor $f(\psi_m)$ in (40) is analogous to the widely recognized factor known as Array Factor (AF) for ULA phased arrays. Note that when ψ is small, $f(\psi_m)$ in (40) can be approximated to:

$$f(\psi_m) = \frac{sin\left(\frac{N\psi_m}{2}\right)}{\frac{\psi_m}{2}} = \frac{sin\left(\frac{\pi Nd}{\lambda}cos\,\phi_m\right)}{\frac{\pi d}{\lambda}cos\,\phi_m} = N\text{sinc}(w_m) \quad (42)$$

where, $\text{sinc}(w) = \frac{sin\,\pi w}{\pi w}$ is the sinc function and:

$$w_m = \frac{Nd}{\lambda}cos\,\phi_m \quad (43)$$

Fig.3 shows the variation of the normalized $|f_n(\psi_m)| = |f(\psi_m)/f_{max}(\psi_m)| = |f(\psi_m)/N|$ versus d/λ for a six-element receiving ULA-SASPA array with three different azimuth directions, ϕ_m. The figure depicts that $f_n(\psi_m)$ is a function with zero crossings at $\frac{r}{(N\,cos\,\phi_m)}$ and can be found by solving:

$$sin\left(\frac{\pi Nd}{\lambda}cos\,\phi_m\right) = 0 \quad \Rightarrow \quad \frac{\pi Nd}{\lambda}cos\,\phi_m = r\pi$$

$$\Rightarrow \quad \frac{d}{\lambda} = \frac{r}{N\,cos\,\phi_m}, \quad r = 1,2,\ldots$$

It is clear from Fig. 3 that, for a given ϕ_m, all values of the scaling factor $f_n(\psi_m)$ are useful except for the points where they are nulls. However, the values of $f_n(\psi_m)$ prior to the first null are the only effective ones, as it exhibits small values beyond this null. Therefore, the range of $f_n(\psi_m)$ until its first null will be taken as the scaling factor. The first null, D, can be determined from the period of $f_n(\psi_m)$, as can be inferred from Fig. 3. Thus, for a given ϕ_m, the first null (FN) occurs at:

$$\left(\frac{d}{\lambda}\right)_{\text{FN}} = D = \frac{1}{N\,cos\,\phi_m} \quad (44)$$

Fig. 3 demonstrates that successful DoA estimation employing ULA-SASPA array for signals arriving from end fire directions requires arrays with a small range of inter-element spacing. The range of spacing $\leq 0.2\lambda$, for example, can be utilized as the range of the inter-element spacing for a six-half-wave dipole ULA-SASPA array to effectively estimate the DoA of signals originating from the directions $0° \leq \phi_i \leq 30°$. However, for directions within the range $\phi_i \geq 60°$, ULA-SASPA arrays with inter-element spacing $0 < d \leq 0.32\lambda$ prove to be beneficial. The inter-element range, $0 < d \leq 0.96\lambda$, is effective for signal directions close to the broadside direction of the array. The first null formula, D, defined in (44), is plotted against azimuth directions, ϕ_m, in Fig.4 for a different number of N. The plot depicts that the scaling factor, $f_n(\psi_m)$, decreases as N increases. This aligns with the observation that more elements in ULA-SASPA arrays have negligible impact, as the mutual coupling effect diminishes between the active element and the remote parasitic elements.

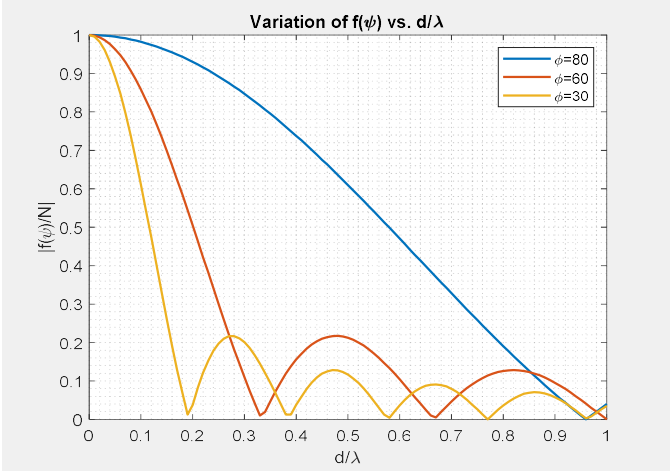

Figure 3: A graph of the normalized scaling factor $|f_n(\psi_m)|$ versus d/λ for various azimuth directions.

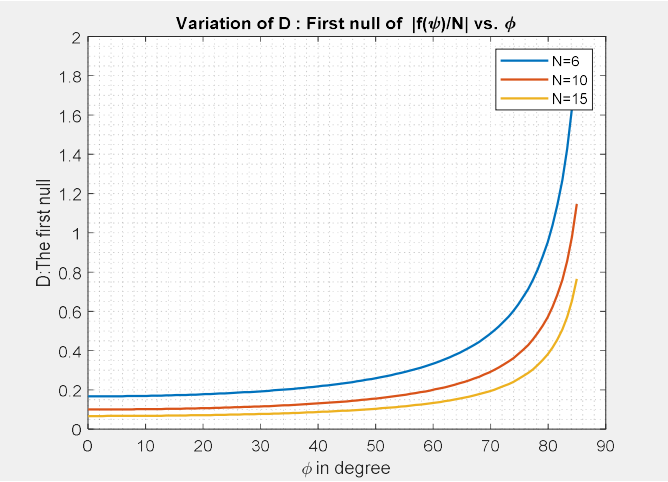

Figure 4: A graph of the first null of $f_n(\psi_m)$, D, against the azimuth direction for various quantities of array antenna elements.

4.2. *Derivation of Eq. 38.*

The derivation of (38) is available in numerous textbooks on Antenna Theory, including [4, 12]. It is provided here for ease. The matrix $\mathbf{G}$ in (27) can be rewritten as:

$$\mathbf{G} = \sum_{n=1}^{N} \mathbf{\Theta}^{n-1} = \sum_{n=0}^{N-1} \mathbf{\Theta}^{n} \tag{45}$$

Where $\mathbf{\Theta}^{n-1}$ is defined in (14). Each term in $\mathbf{G}$ can be rewritten using the geometric series formula as:

$$\sum_{n=0}^{N-1} e^{-jnkd\cos\phi_m} = \frac{1-e^{-jNkd\cos\phi_m}}{1-e^{-jkd\cos\phi_m}}$$

$$= \frac{e^{-j0.5Nkd\cos\phi_m}}{e^{-j0.5kd\cos\phi_m}} \times \frac{e^{+j0.5Nkd\cos\phi_m} - e^{-j0.5Nkd\cos\phi_m}}{e^{+j0.5kd\cos\phi_m} - e^{-j0.5kd\cos\phi_m}}$$

$$= e^{-j0.5(N-1)kd\cos\phi_m} \frac{sin(0.5Nkd\cos\phi_m)}{sin(0.5kd\cos\phi_m)} \tag{46}$$

which results the elements of $\mathbf{G}$ in (38). If the array is arranged symmetrically around the origin, then the factor $exp(-j0.5(N-1)kd\cos\phi_m)$ can be removed [12]. i.e.:

$$\mathbf{G} = \text{diag}\left(\frac{sin\left(\frac{N}{2}kd\cos\phi_1\right)}{sin\left(\frac{1}{2}kd\cos\phi_1\right)}, \ \ldots, \ \frac{sin\left(\frac{N}{2}kd\cos\phi_M\right)}{sin\left(\frac{1}{2}kd\,co\quad_M\right)}\right) \tag{47}$$

4.3. *Simulations Study.*

To demonstrate the effectiveness of ULA-SASPA arrays and their improvement in estimating the DoAs of received signals even with small spacing between the array's elements, the following simulation scenarios were performed. The improvements will be illustrated by contrasting the performance of an array in SASPA mode versus when it is all-active. The simulations are conducted for measurements that are free from mutual coupling, assuming that this effect has been removed beforehand. Moreover, the restrictions on the range of inter-element spacing based on azimuth directions, as discussed in Section 4.1, will be demonstrated. Fig.5a shows how a ULA-SASPA array can estimate two signals originating from the directions $\phi_1 = 79°$ and $\phi_2 = 82°$ by using the noise subspace, $\hat{\mathbf{E}}_{n,ULA-SASPA}$, which is estimated from the array's measurements. The array consists of six half-wave dipole elements, with the spacing between the elements being $d = 0.15\lambda$. The signal to noise ratio of the received signals is SNR = 40 dB. Fig.5b depicts the MUSIC spectrum for the same scenario, but the array is all-active. In Fig.6, the MUSIC spectra are shown for the same scenario as Fig.5, but with smaller inter-element spacing: $d = 0.12\lambda$. However, the SNR of the received signals is increased to 45 dB. The two figures clearly illustrate that the DoA estimation using a ULA-SASPA array is achieved with high resolution, despite the array aperture being small and the received signals being spatially very close to one another, whereas the ULA all-active array was unable to estimate the DoA of the same received signals.

Other simulations are shown in Fig.7. The same array employed previously to obtain Fig.5 is used again, but the signals are now coming from azimuthal directions $\phi_1 = 30°$ and $\phi_2 = 35°$. However, a higher SNR of the received signal and a greater number of measurement snapshots than in the previous simulations were required to achieve a good DoA estimation. The reason is that the signals are incoming from the end fire direction of the array. Fig.8 shows that when $d = 0.19\lambda$, the resolution of the estimated DoAs, which are $\phi_1 = 40°$ and $\phi_2 = 44°$, using a ULA-SASPA array is poor, resulting in another erroneous detection. This occurs due to a violation the condition in (44). Fig.9 displays a comparison between the RMSE values obtained for a signal coming from the direction $\phi_1 = 10°$ and received by ULA-SASPA and ULA all-active arrays. Each array consists of four half-wave dipole elements with $d = 0.15\lambda$. It is clearly evident from this figure that the RMSE values for the signal received by a ULA-SASPA array is much less than the RMSE values for the signal when received by the all-active antenna array. Thus, the estimated DoA is very close to the true values over a wide range of SNR when using a ULA-SASPA array.

The improvements depicted in the aforementioned simulation outcomes stem from the inherent phenomena provided by the SASPA array. These phenomena lead to a scaling matrix, which in turn, produces a factor represented by $f(\psi_m)$ that offers a gain to the received signal. Nonetheless, the price for this enhancement for ULA-SASPA arrays is the requirement for the proper selection of inter-element spacing for a specific azimuth sector to ensure effective DoA estimation.

4.4 *UCA-SASPA Array.*

In the next section, it will be shown that the matrix $\mathbf{X} = \left(\sum_{n=1}^{N} \mathbf{\Psi}^{(n)}\right)$, which scales the steering matrix of a UCA-SASPA array, can be simplified to:

$$\mathbf{X} = diag[N\Sigma_{t=0}^{\infty}(-j)^{tN}\zeta J_{tN}(kR)cos(tN\phi_1), \cdots, N\Sigma_{t=0}^{\infty}(-j)^{tN}\zeta J_{tN}(kR)cos(tN\phi_M)] \quad (48)$$

The factor $J_v(x)$ represents the Bessel function of the first kind of order *v*, while *R* is the radius of the array, and

$$\zeta = \begin{cases} 1, & t = 0 \\ 2, & t \neq 0 \end{cases}$$

The Bessel functions as a function of *x* is shown in Fig.10. The figure illustrates that for orders > 6 , where v is an integer, the Bessel functions exhibit small amplitudes when *x* is increased. Therefore, the range $v \leq 6$ may be the only useful range for determining the infinite summations in (48). This means that the values $t = 0$ and 1 will be used only. Additionally, the term $(-j)^{tN}$ will take the value ± 1, as long as *N* is even. Accordingly, the summation terms in (48) remain real because of symmetry. However, the summation terms will be complex if *N* is odd. As an example, $J_0(x)$ and $J_6(x)$ are the only significant amplitudes in the case of a six-half-wave dipole UCA-SASPA array. However, $J_6(x)$ is much smaller than $J_0(x)$. Consequently, the scaling factor for this example will be $NJ_0(x)$, which in turn, is not ϕ_m dependent. As a result, $NJ_0(x)$ will scale the rotation matrix $\mathbf{T}_{UCA-SASPA}$ in (33) for signals received regardless their azimuth directions. Accordingly, the distance measure between the steering matrix $\mathbf{U}_{UCA}$ and the estimated signal subspace $\hat{\mathbf{E}}_{s,UCA-SASPA}$ will be reduced. Based on this, the useful range of radii of UCA-SASPA arrays for accurate and improved DoA estimation can be determined from the first null of $J_0(x)$. Fig.10 clearly shows that this first null occurs at $x = kR \approx 2.5$. The range $kR < 2$, meaning $R < \lambda/\pi$, can be taken as a useful range so that only $J_0(x)$ will be the approximated result of the summation in (48).

4.5 *Derivation of the Elements of X in Eq. 48.*

Recall the matrices $\mathbf{X} = \sum_{n=1}^{N} \mathbf{\Psi}^{(n)}$ and $\mathbf{\Psi}^{(n)}$presented in (31) and (18), respectively. Each term in $\mathbf{X}$ can be rewritten using the Jacobi-Anger expansion [5]:

$$\sum_{n=1}^{N} e^{-jkR\,cos\left(\phi_m - 2\pi\frac{n-1}{N}\right)} = \sum_{1}^{N}\sum_{v=-\infty}^{\infty}(-j)^v J_v(kR) e^{jv\left(\phi_m - 2\pi\left(\frac{n-1}{N}\right)\right)} \quad (49)$$

The factor $J_v(x)$ represents the Bessel function of the first kind of order *v*. The expression in (49) can be simplified further as:

$$\sum_{n=1}^{N} e^{-jkR\,c\,\left(\phi_m - 2\pi\frac{n-1}{N}\right)} = \sum_{v=-\infty}^{\infty}(-j)^v J_v(kR)\, e^{jv\phi_m} \sum_{1}^{N} e^{-j2\pi\frac{(n-1)v}{N}} \quad (50)$$

Now

$$\sum_{1}^{N} e^{-j2\pi\frac{(n-1)v}{N}} = \sum_{0}^{N-1} e^{-j2\pi\frac{nv}{N}} = \begin{cases} N & v = 0, \pm tN \quad t = 1,2,\ldots \\ 0 & \text{otherwise} \end{cases} \quad (51)$$

Therefore, (50) becomes:

$$\sum_{n=1}^{N} e^{-jkR\,cos\left(\phi_m - 2\pi\frac{n-1}{N}\right)} = N\sum_{t=-\infty}^{\infty}(-j)^{tN} J_{tN}(kR) e^{jtN\phi_m} = N\sum_{t=0}^{\infty}(-j)^{tN}\zeta J_{tN}(kR)\, cos(tN\phi_m)$$
$$\zeta = 1 \quad t = 0$$
$$\zeta = 2 \quad t \neq 0 \quad (52)$$

4.6 *Simulations Study.*

The subsequent simulations were conducted to verify the capability of UCA-SASPA arrays to function successfully as direction-finding arrays. The radius of the array used in these simulations is selected from the range $R < \lambda/\pi$, as discussed in section 4.3. It will be shown that UCA-SASPA arrays with such a range of radii can successfully estimate the DOA for incoming signals with very high resolution, regardless of the signals' various azimuth directions and their spatial closeness. Fig.11 shows the MUSIC spectrum obtained by using the $\hat{\mathbf{E}}_{n,UCA-SASPA}$ and the scaling factor (52) in (36). The array consists of six half-wave dipole antennas and with a radius, $R = 0.2\lambda$. The array is receiving two signals coming from the directions $\phi_1 = 79°$ and $\phi_2 = 83°$ with SNR $= 40$ dB. As a comparison, the DoA estimation of the same signals received by a six half-wave

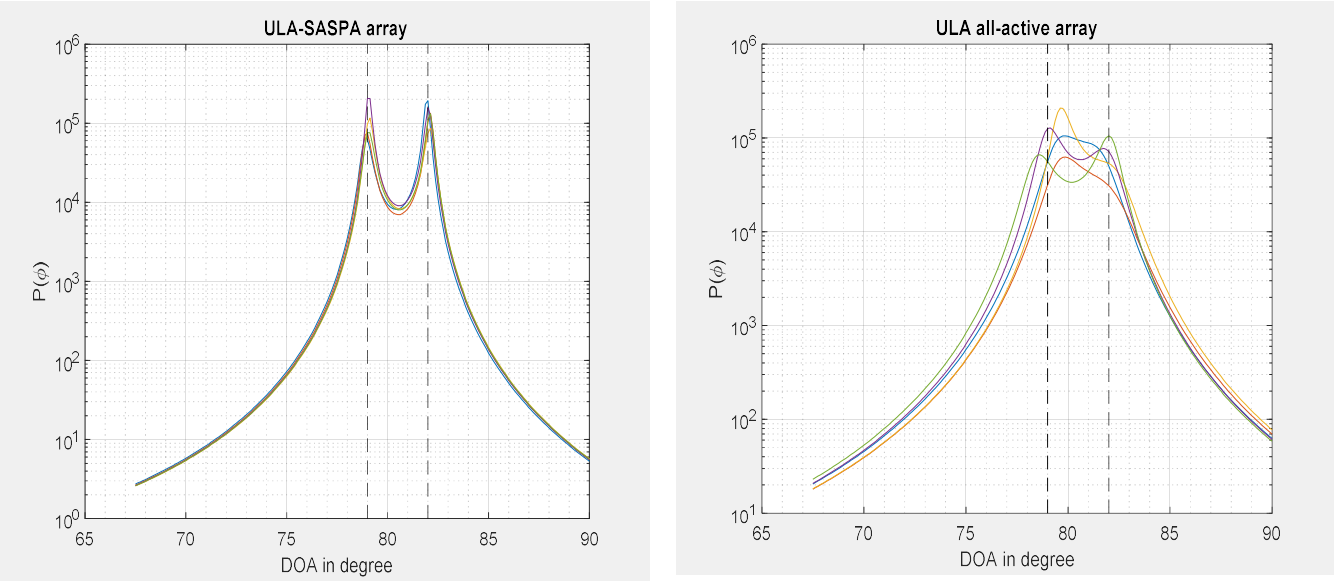

(a) (b)

Figure 5: MUSIC spectra for two incoming signals from the directions $\phi_1 = 79°$ and $\phi_2 = 82°$, received by a ULA array consisting of six half-wave dipoles. The inter-element spacing is $d = 0.15\lambda$. Each signal is received with a SNR $= 40$ dB. A total of 1000 measurement snapshots were used. (a) Using ULA-SASPA array. (b) Using ULA all-active array.

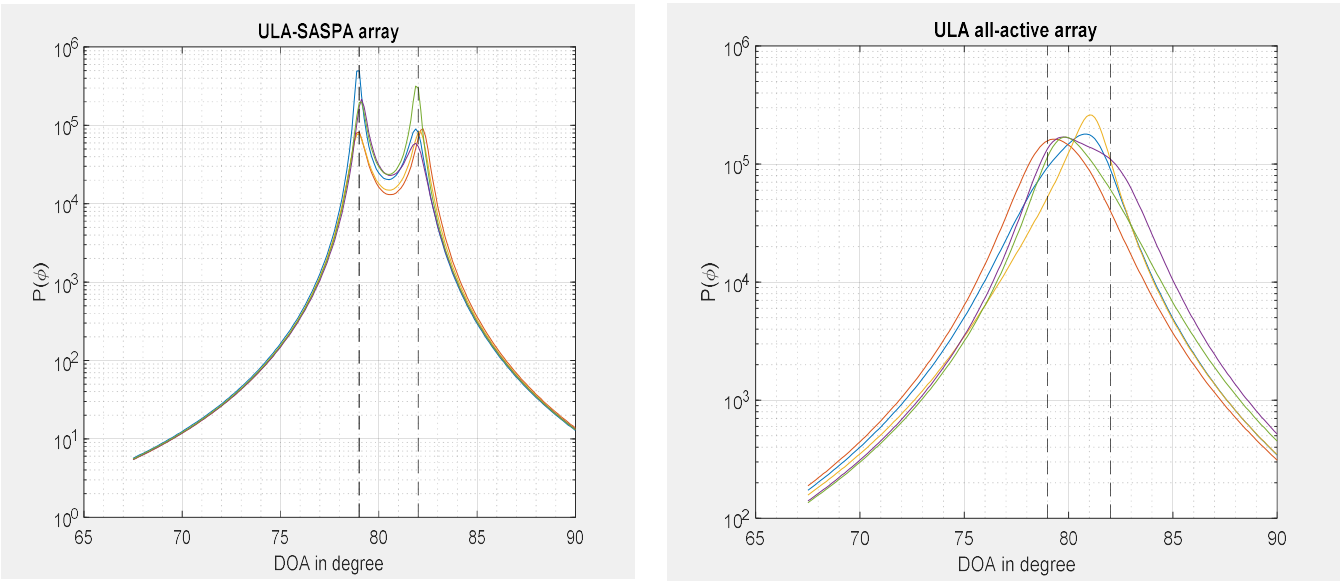

(a) (b)

Figure 6: MUSIC spectra for two incoming signals from the directions $\phi_1 = 79°$ and $\phi_2 = 82°$, received by a ULA array consisting of six half-wave dipoles. The inter-element spacing is $d = 0.12\lambda$. Each signal is received with a SNR $= 45$ dB. A total of 1000 measurement snapshots were used. (a) using ULA-SASPA array. (b) using ULA all-active array.

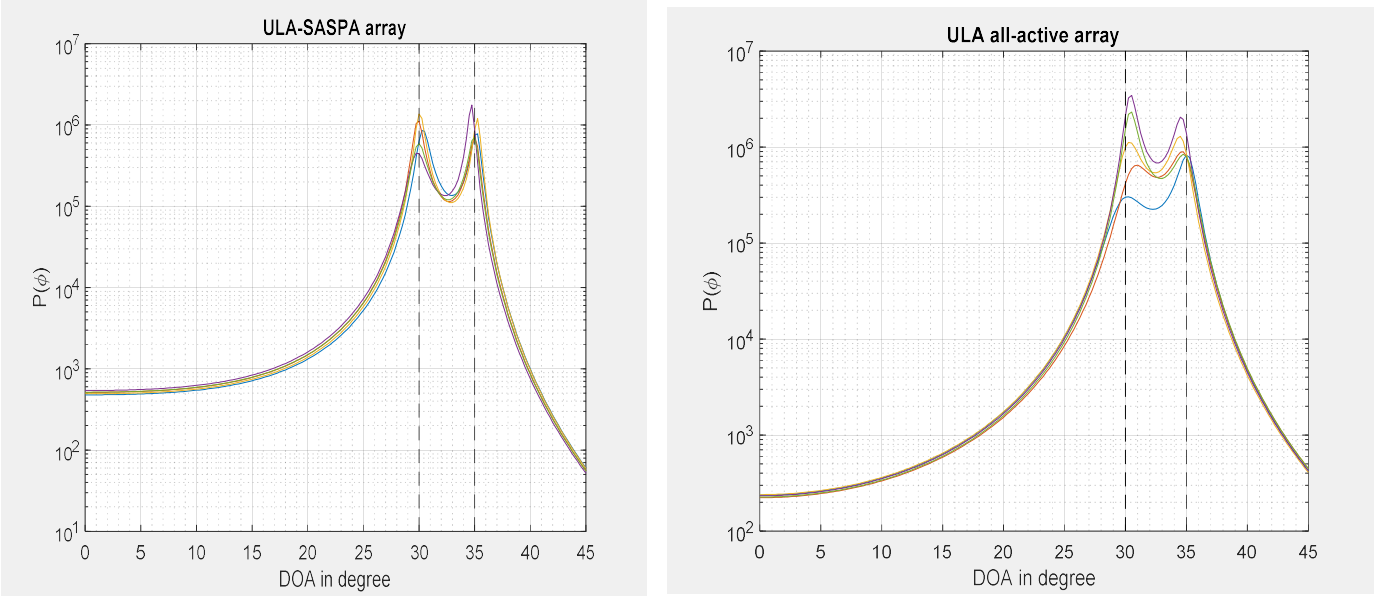

(a) (b)

Figure 7: MUSIC spectra for two signals coming from the directions $\phi_1 = 30°$ and $\phi_2 = 35°$, received by a ULA array consisting of six half-wave dipoles. The inter-element spacing is $d = 0.15\lambda$. Each signal is received with a SNR $= 50$ dB. A total of 2000 measurement snapshots were used. (a) using ULA-SASPA array. (b) using ULA all-active array.

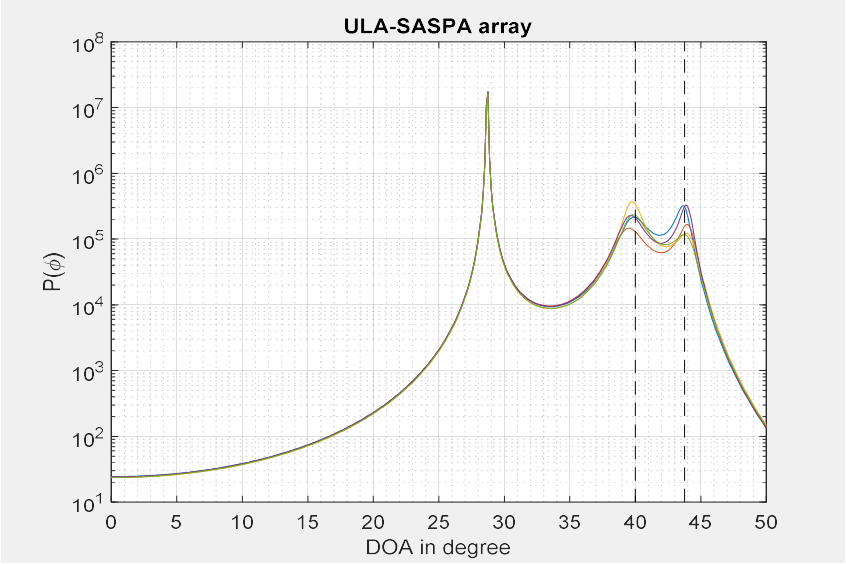

Figure 8: A plot shows the MUSIC spectrum for two incoming signals from the directions $\phi_1 = 40°$ and $\phi_2 = 44°$, received by a ULA-SASPA array. The array consists of six half-wave dipoles with inter-element spacing $d = 0.19\lambda$. The plot shows an erroneous detection due to d being nearly equal to the first null of $f_n(\psi_m)$.

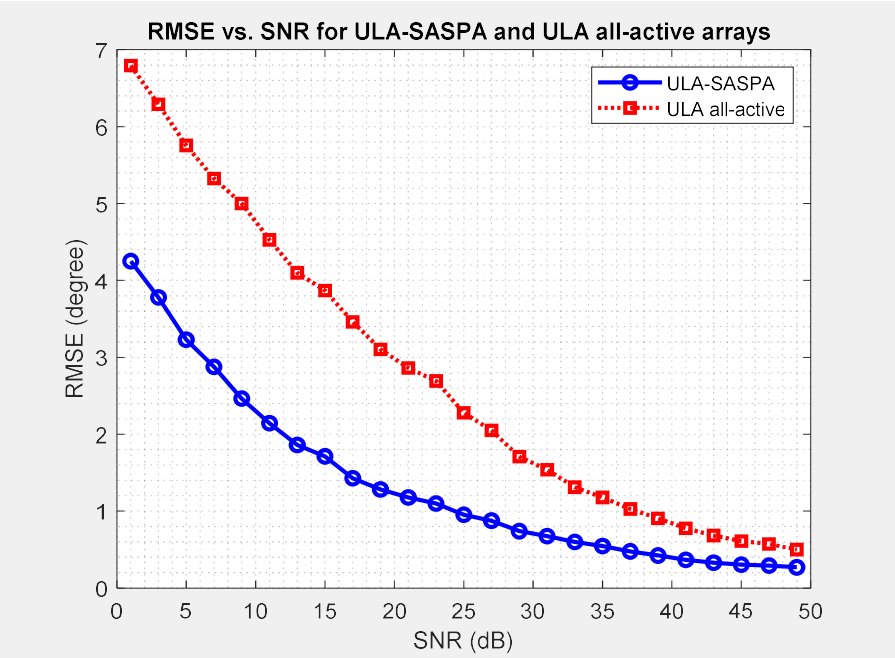

Figure 9: RMSE plots for a signal coming from the direction $\phi_1 = 10°$ and incident on ULA-SASPA and ULA all-active antenna arrays. Each array consists of four half-wave dipoles with inter-element spacing $d = 0.15\lambda$.

dipole UCA all-active antenna array with the same radius, is also included in the figure. Evidently, the UCA-SASPA array, with a compact size, was effective in accurately estimating the signals' DoA with high resolution. Conversely, the UCA all-active array cannot differentiate the DoA of the incoming signals.

The simulation shown in Fig.12 confirms the ability of the UCA-SASPA array to efficiently estimate the DoA of incoming signals from critical directions (end fire), as discussed earlier. The same array used for Fig.11 is employed to estimate the DoA of the signals coming from the azimuth directions $\phi_1 = 30°$ and $\phi_2 = 34°$. The signals are also received with the same SNR as before. Thus, in addition to being direction finding arrays with high resolution, like ULA-SASPA arrays, compact-sized UCA-SASPA arrays have the capability to detect the DoA of signals irrespective of their directions. In Fig.13, the RMSE criterion is investigated for a signal coming from the azimuth direction $\phi_1 = 10°$ and received by UCA-SASPA and UCA all-active arrays. Each array consists of four half-wave dipoles with a radius equal to $R = 0.2\lambda$. This figure clearly shows that the difference between the true and estimated values of the DoA using the UCA-SASPA array is very small compared to the UCA all-active array.

It is worth mentioning that the preceding simulations confirm the superiority of UCA arrays over ULA arrays. The simulations showed that UCA-SASPA arrays offer inherently useful characteristics: symmetry and unambiguity, as they successfully estimate the incoming signals with high resolution, regardless of the directions of these signals. On the other hand, it is necessary to adjust certain parameters, such as SNR or inter-element spacing, to successfully detect the DoA of incoming signals when using ULA-SASPA arrays.

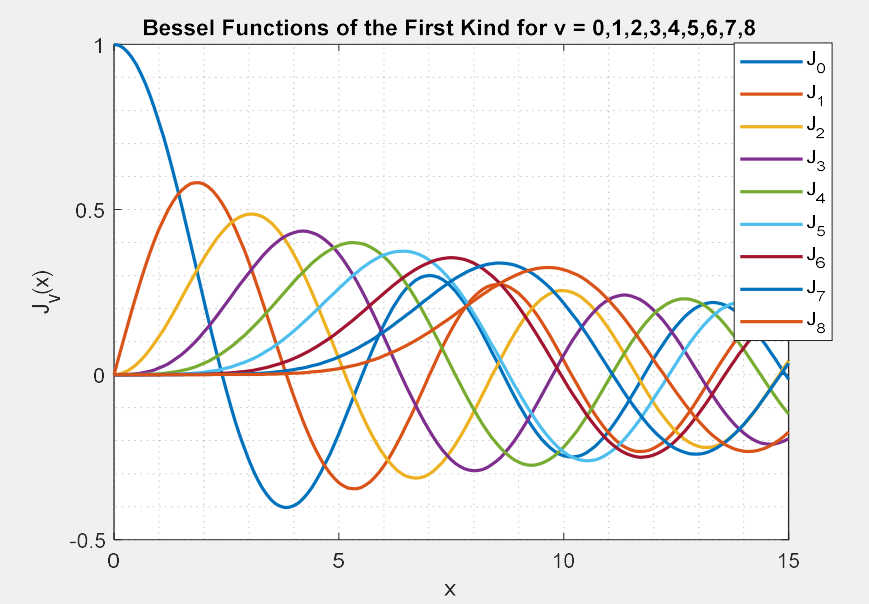

Figure 10: Bessel functions of the first kind for different order *v*.

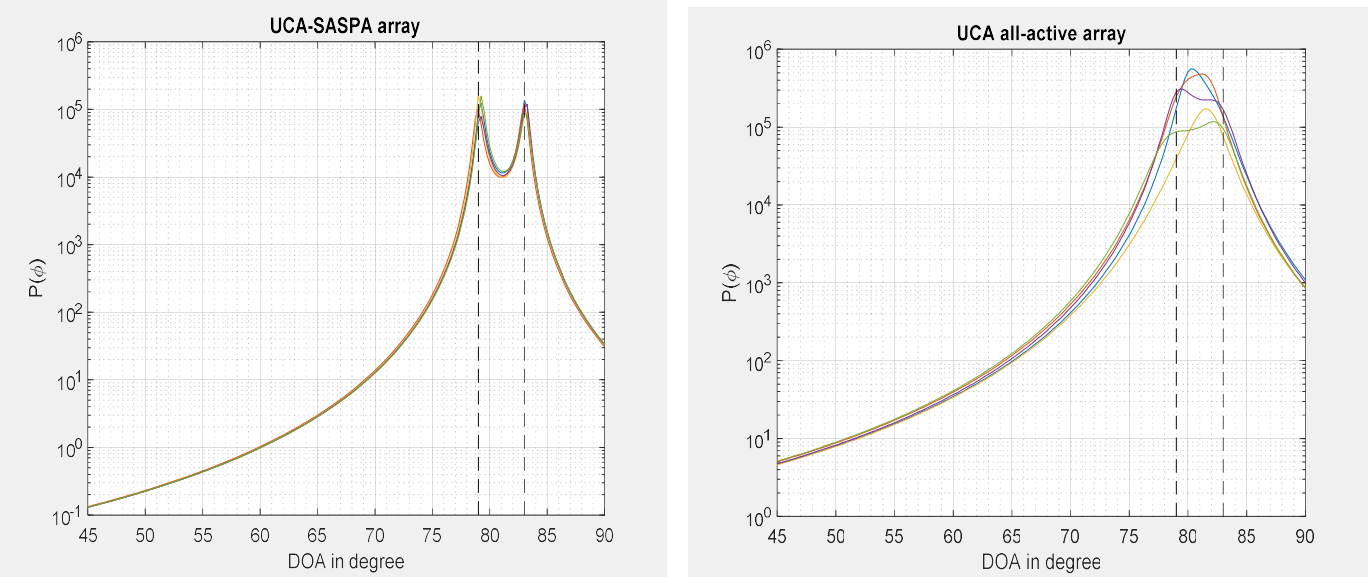

(a) (b)

Figure 11: MUSIC spectra for two incoming signals from the directions $\phi_1 = 79°$ and $\phi_2 = 83°$, incident on a UCA antenna array consisting of six half-wave dipoles with a radius $R = 0.2\lambda$. Each signal is received with a SNR = 40 dB. A total of 1000 measurement snapshots were used. (a) using UCA-SASPA array. (b) using UCA all-active array.

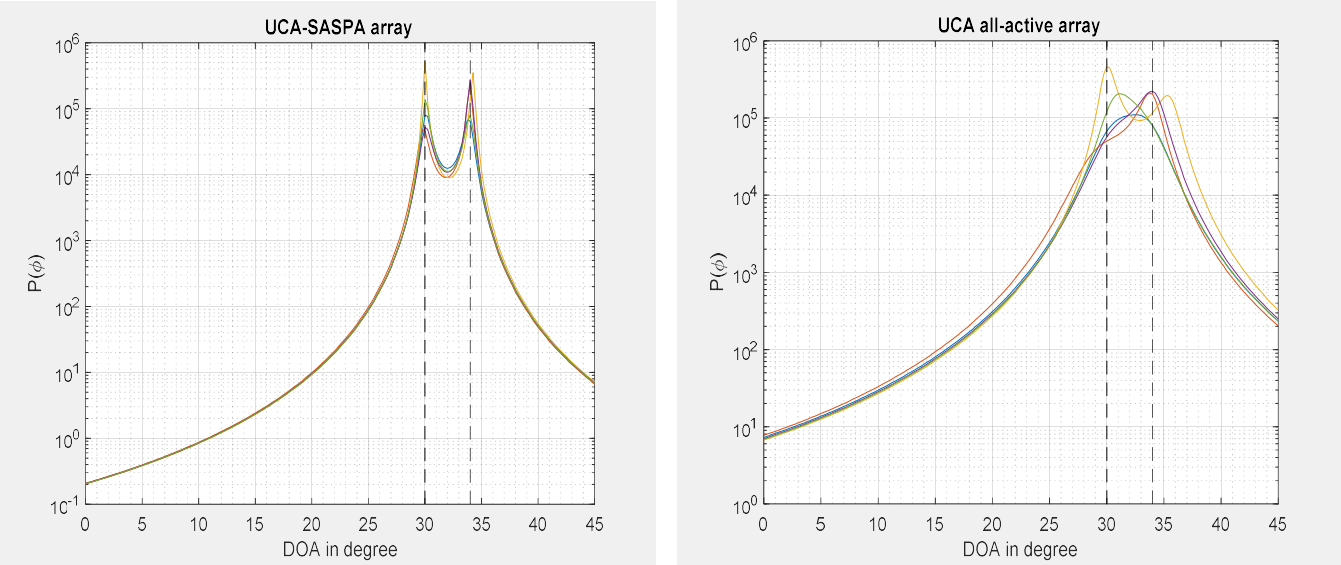

(a) (b)

Figure 12: MUSIC spectra for two incoming signals from the directions $\phi_1 = 30°$ and $\phi_2 = 34°$, incident on a UCA antenna array consisting of six half-wave dipoles with a radius $R = 0.2\lambda$. Each signal is received with a SNR = 40 dB. A total of 1000 measurement snapshots were used. (a) using UCA-SASPA array. (b) using UCA all-active array.

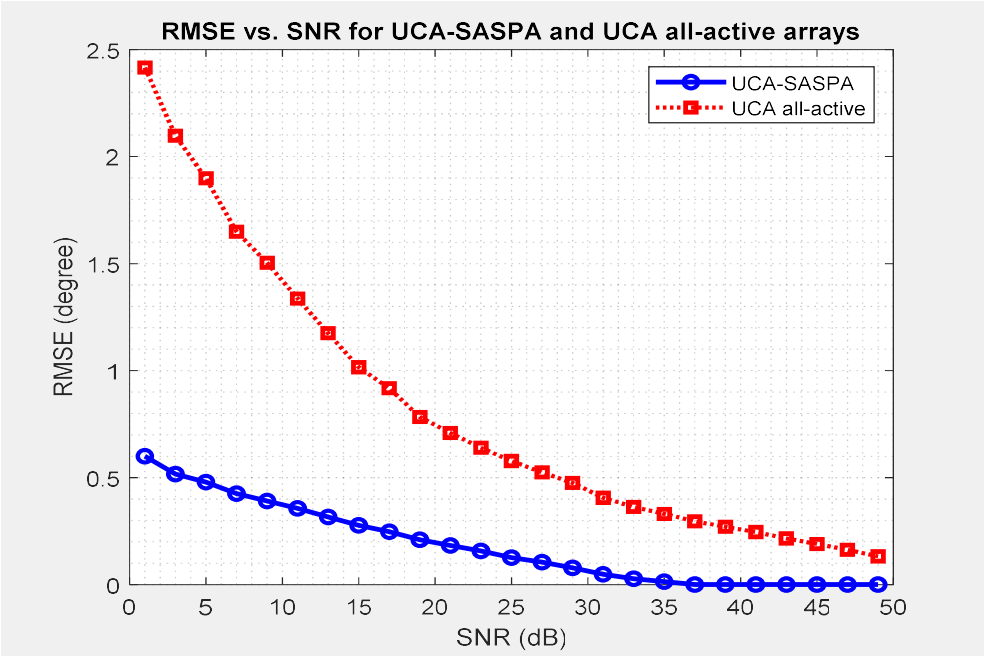

Figure 13: RMSE plots for a signal coming from the direction $\phi_1 = 10°$ and impinging on UCA-SASPA and UCA all-active arrays. Each array consists of four half-wave dipoles with a radius $R = 0.2\lambda$.

5. The effect of The PIN Diode and The Practical Consideration.

The vector $\mathbf{y}^{(n)}(t)$ in (2) is a zero vector except for the entry corresponding to the active element. Practically, this can be implemented by developing the measurement on the terminal of only one loaded antenna element in the SASPA array. When the terminals of a dipole antenna are connected across a load Z_L , the element becomes active. Short-circuiting the terminals of the element converts it to a parasitic element. This functionality can be achieved in microwave circuits with the aid of using RF switches, such as FET switches, PIN switches, and MEMS switches [7]. PIN diodes are widely used as RF switches because of their linearity, very low insertion loss, being cheap, very fast switching and low-ON state and high-OFF state impedance [2, 7, 9]. Fig. 14 shows a practical circuit using two PIN diodes to switch an antenna between active and parasitic states. The circuit is Single-Pole-Double-Throw (SPDT). Using two PIN diodes as in this figure provides a perfect isolation between the active and parasitic states. Two of these circuits may be used between the two halves of a dipole antenna, while one circuit is sufficient if the antenna is a monopole. The load is connected between the two RF port 1s of the circuits, and the two RF port 2s are short-circuited. The two halves of the dipole are connected between the two RF port3s. When the diodes D1 are forward-biased and the diodes D2 are reverse-biased, the element is in the active state. When the diodes D2 are forward biased and the diodes D1 are reverse-biased, the element is in the parasitic state. RF switches using circuits with series PIN diodes are better than using shunt PIN diodes [2].

The forward resistance (The ON state) of the PIN diode is equal to or less than 1Ω. The OFF state of the PIN diodes is normally greater than $100K\Omega$, which is the diode capacitance. The effect of these values when added with the equivalent circuit's impedance will result in minimal effect if the type of the PIN diodes is carefully chosen to operate with the operating band of frequencies. In [2], it is pointed out that the biasing conditions have negligible effect on the antenna radiation pattern. However, the OFF state may affect the input impedance of the related antenna element. As a future work, the drawbacks of using the PIN diodes as RF switch on the DoA estimation capability of an antenna array may be studied.

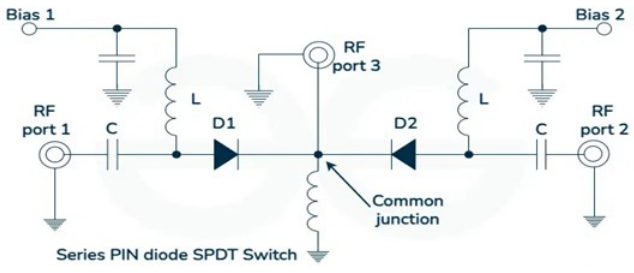

https://www.geeksforgeeks.org/pin-diode/

Figure 14: A practical SPDT circuit using two PIN diodes.

6. Conclusion.

The advantages of ULA-SASPA and UCA-SASPA as DoA estimation arrays have been explored in this study. It was verified that ULA-SASPA and UCA-SASPA arrays are capable of estimating the DoAs of received signals with a resolution much better than that of traditional antenna arrays, which consist of elements that are all in an active state. The benefits of SASPA arrays stem from scaling the steering matrix of the measurements of antenna array by a unitary matrix when receiving signals. The unitary matrix arises from the additional spatial phase shift that occurs to the received signal due to the retransmission from the parasites into the active element. However, certain restrictions apply to selecting the inter-element spacings of the array to avoid cases where the elements of the unitary matrix may have small values. The very small values of RMSE calculations also confirm the capability of SASPA as direction-finding arrays with very high resolution compared to all-active antenna arrays. It was also shown that the performance of the UCA-SASPA array is superior to that of the ULA-SASPA array under the same conditions.

References

[1] A. Kausar, H. Mehrpouyan, M. Sellathurai, R. Qian, and S. Kausar, "Energy efficient switched parasitic array antenna for 5G networks and IoT," in *2016 Loughborough Antennas & Propagation Conference (LAPC)*, 14-15 Nov. 2016, pp. 1-5, doi: http://doi.org/10.1109/LAPC.2016.7807569 .

[2] B. Boyapati and K. Jayendra, "Effect of PIN Diode Integration on Patch Antennas for Frequency Reconfigurable Antenna Applications," *Advances in Technology Innovation,* vol. 8, no. 3, pp. 210-218, 07/0 ,2023 doi: 10.46604/aiti.2023.9235.

[3] B. R. Jackson, S. Rajan, B. J. Liao and S. Wang, "Direction of Arrival Estimation Using Directive Antennas in Uniform Circular Arrays," in *IEEE Transactions on Antennas and Propagation*, vol. 63, no. 2, pp. 736-747, Feb. 2015, doi: 10.1109/TAP.2014.2384044.

[4] C. A. Balanis, *Antenna theory: Analysis and design*, 4th ed. John Wiley & Sons, 2016.

[5] C. A. Balanis, *Advanced Engineering Electromagnetics*, 2nd ed. John Wiley & Sons, Inc., 2012.

[6] D. V. Thiel and S. Smith, *Switched Parasitic Antennas for Cellular Communications*. Artech House, Inc., 2001.

[7] J. Kumar, B. Basu, and F. Talukdar, "Modeling of a PIN Diode RF Switch for Reconfigurable Antenna Application," *Scientia Iranica,* 01/13 2018, doi: 10.24200/sci.2018.20110.

[8] J. K. Ji, "Compact dual-band pattern reconfigurable antenna using switched parasitic array," *Electronics*

Letters, vol. 53, no. 4, pp. 211-212, 2017, doi: https://doi.org/10.1049/el.2016.3486.

[9] J.-N. Lee, Y.-H. Lee, K.-C. Lee, and T. Joong Kim, "Passive parasitic UWB antenna capable of switched beam-forming in the WLAN frequency band using an optimal reactance load algorithm," *ETRI Journal,* vol. 41, no ,6 .pp. 715-730, 2019, doi: https://doi.org/10.4218/etrij.2018-0393.

[10] J. Yuan, H. Xiao, Z. M. Cai, and C. Xi, "DOA estimation based on multiple beamspace measurements sparse reconstruction for manoeuvring towed array," *Journal of Physics: Conference Series,* vol. 787, no. 1, p. 012026, 2017/01/01 2017, doi: 10.1088/1742-6596/787/1/012026.

[11] K. Chen, W. Jin, and B. Desikan, "A Signal Subspace Rotation Method for Localization of Multiple Wideband Sound Sources," *ArXiv,* vol. abs/1906.08847, 2019.

[12] K. Kishore, *Antenna and wave propagation*. New Delhi: I.K. International Publishing House. Pvt. Ltd, 2009.

[13] K. Vinayagam and R. Natarajan, "Polarization Reconfigurable Patch Antenna Using Parasitic Elements for Sub–6 GHz Applications," *International Journal of Electrical and Computer Engineering Systems,* vol. 16, no. 1, pp. 1-7, 12/09 2024, doi: 10.32985/ijeces.16.1.1.

[14] K. Zhao, F. Liu, W. Chen, and Z. Feng, "Bandwidth-enhanced of a planar switched parasitic array antenna," in *2010 International Conference on Microwave and Millimeter Wave Technology*, 2010, pp. 1129-1131, doi: http://doi.org/10.1109/ICMMT.2010.5525078 .

[15] L. Reinhold, C. Wasle, and A. Kölpin, "A circular switched parasitic array with directors for LoRa applications at 868 MHz," *Electronics Letters,* vol. 60, 2024, doi: http://doi.org/10.1049/ell2.13247.

[16] M. A. Towfiq, I. Bahceci, S. Blanch, J. Romeu, L. Jofre, and B. A. Cetiner, "A Reconfigurable Antenna With Beam Steering and Beamwidth Variability for Wireless Communications," *IEEE Transactions on Antennas and Propagation,* vol. 66, no. 10, pp. 5052-5063, 2018, doi: http://doi.org/10.1109/TAP.2018.2855668.

[17] M. L. McCloud and L. L. Scharf, "A new subspace identification algorithm for high-resolution DOA estimation," *IEEE Transactions on Antennas and Propagation,* vol. 50, no. 10, pp. 1382-1390, 2002, doi: http://doi.org/10.1109/TAP.2002.805244.

[18] M. R. Kamarudin and P. Hall, "Switched beam antenna array with parasitic elements," *Progress in Electromagnetics Research B,* vol. 13 ,pp. 187-201, 2009, doi: http://doi.org/10.2528/PIERB09011603.

[19] M. Shaghaghi and S. A. Vorobyov, "Subspace Leakage Analysis and Improved DOA Estimation With Small Sample Size," *Trans. Sig. Proc.,* vol. 63, no. 12, pp. 3251–3265, 2015, doi: http://doi.org/10.1109/tsp.2015.2422675.

[20] M. Wennstrom and T. Svantesson, "An antenna solution for MIMO channels: the switched parasitic antenna," in *12th IEEE International Symposium on Personal, Indoor and Mobile Radio Communications. PIMRC 2001. Proceedings (Cat. No.01TH8598)*, 2001, vol. 1, doi: http://doi.org/10.1109/PIMRC.2001.965412 .

[21] P. Chaipanya, "Low profile switched beam utilizing a ring-parasitic antenna," in *2015 International Symposium on Antennas and Propagation (ISAP)*, 9-12 Nov. 2015, pp. 1-4.

[22] P. K. Pal and R. S .Sherratt, "MIMO Channel Capacity and Configuration Selection for Switched Parasitic Antennas," *ETRI Journal,* vol. 40, no. 2, pp. 197-206, 2018, doi: https://doi.org/10.4218/etrij.2017-0071.

[23] P. K. Varlamos and C. N. Capsalis, "Direction-of-Arrival Estimation (DoA) Using Switched Parasitic Planar Arrays and the Method of Genetic Algorithms," *Wireless Personal Communications,* vol. 28, no. 1, pp. 59-75, 2004, doi: http://doi.org/10.1023/B:WIRE.0000015382.62938.1c.

[24] R. A. Jasem, "High Resolution Direction of Arrival Estimation with Switched Active Switched Parasitic Antenna Arrays," Ph.D. dissertation, Curtin University, Perth, 2020.

[25] R. Roy and T. Kailath, "ESPRIT-estimation of signal parameters via rotational invariance techniques ", *IEEE Transactions on Acoustics, Speech, and Signal Processing,* vol. 37, no. 7, pp. 984-995, 1989, doi: http://doi.org/10.1109/29.32276.

[26] S. C. Panagiotou, S. C. A. Thomopoulos, and C. N. Capsalis, "Genetic Algorithms in Antennas and Smart Antennas Design Overview: Two Novel Antenna Systems for Triband GNSS Applications and a Circular Switched Parasitic Array for WiMax Applications Developments with the Use of Genetic Algorithms," *International Journal of Antennas and Propagation,* vol. 2014, no. 1, p. 729208, 2014, doi: https://doi.org/10.1155/2014/729208.

[27] T. Bertuch, R. Joseph, and K. Herbertz, "Size-Limited Q-Band Circular Switched Parasitic Array Antenna With Small Elevation Beamwidth," *IEEE Transactions on Antennas and Propagation,* vol. 63, no. 11, pp. 4749-4758, 2015, doi: 10.1109/TAP.2015.2477516.

[28] T. Svantesson and M. Wennstrom, "High-resolution direction finding using a switched parasitic antenna," in *Proceedings of the 11th IEEE Signal Processing Workshop on Statistical Signal Processing (Cat. No.01TH8563)*, 2001, pp. 508-511, doi: http://doi.org/10.1109/SSP.2001.955334 .

[29] T. Svantesson, "Direction Finding in the Presence of Mutual Coupling," Thesis for the degree of Licentiate of Engineering, Department of Signals and Systems, School of Electrical and Computer Engineering, Chalmers University of Technology, Sweeden, 1991 .

[30] V. V. Khairnar, B. V. Kadam, C. K. Ramesha, and L. J. Gudino, "A reconfigurable parasitic antenna with continuous beam scanning capability in H-plane," *AEU - International Journal of Electronics and* Pattern," *IEEE Transactions on Antennas and Propagation,* vol. 55, no. 6, pp. 1883-1887, 2007, doi: http://doi.org/10.1109/TAP.2007.898643.

[32] Y. Jeong, H. Kim, B.-S. Kim, and H. Choo, "Avoidance of Co-channel Interference Using Switched Parasitic Array Antenna in Femtocell Networks," in *Computational Science and Its Applications – ICCSA 2010*, Berlin, Heidelberg, D. Taniar, O. Gervasi, B. Murgante, E. Pardede, and B. O. Apduhan, Eds., 2010: Springer Berlin Heidelberg, pp. 158-167 .

[33] Y. Xu, Y. Huang, S. Shi, K. Zhao, and Z. Liu, "Aligned Subspace Rotation Approach to Parameter Estimation of Wideband Source Signals," presented at the Proceedings of the 2019 International Symposium on Signal Processing Systems, Beijing, China, 2019. [Online]. Available: https://doi.org/10.1145/3364908.3364912.

[34] Z. Imran and C. Panagamuwa, "Beam-switching planar parasitic antenna array," in *2014 Loughborough Antennas and Propagation Conference (LAPC)*, 10-11 Nov. 2014, pp. 160-164, doi: http://doi.org/10.1109/LAPC.2014.6996346 .

[35] Z. Liu, Z. Huang, F. Wang, and Y. Zhou, "DOA estimation with uniform linear arrays in the presence of mutual coupling via blind calibration," *Signal Processing,* vol. 89, no. 7, pp. 1446-1456, 2009, doi: https://doi.org/10.1016/j.sigpro.2009.01.017

Communications, vol. 88, pp. 78-86, 2018, doi: https://doi.org/10.1016/j.aeue.2018.02.014.

[31] W. H. Chen *et al.*, "A Novel Planar Switched Parasitic Array Antenna With Steered Conical

تحديد اتجاه الموجات الكهرومغناطيسية بدقة عالية باستغلال الطور المكاني الاضافي المتكون في المصفوفات الهوائية المستلمة لهذه الموجات والمتضمنة هوائي فعال وهوائيات طفيلية متبادلة.

رباح عبد الجبار جاسم

المعهد التقني في الدور,الجامعة التقنية الشمالية,صلاح الدين , العراق

* *الباحث الممثل: رباح عبد الجبار جاسم* rabah_alobaidi5@yahoo.com , rabah.aj@ntu.edu.iq

نشر في: 31 كانون الأول 2025

الخلاصة – سيُبحث في هذا العمل فائدة إحداث طور مكاني إضافي للإشارات المُستقبَلة بواسطة مصفوفة هوائيات تتضمن هوائي فعال وهوائيات طفيلية متبادلة (SASPA). تنتج هذه المصفوفات طور مكاني للاشارات المستقبلة ، بالإضافة إلى الاطوار المكانية التي تتعرض لها هذه الإشارات عند مرورها عبر مصفوفة هوائيات. هذا الطور الاضافي يحسن دقة تقدير اتجاه الوصول (DoA) بشكل كبير. يحدث هذا الطور الاضافي بصورة متأصلة عند تحويل كل هوائي في مصفوفة SASPA من الحالة الطفيلية إلى الحالة االفعالة مع ترك الهوائيات الأخرى في حالة طفيلية في وقت واحد. يعود هذا التحسن نتيجة توسيع نطاق مصفوفة التوجيه لقياسات مصفوفة SASPA المُستقبِلة بواسطة مصفوفة أحادية. بالتالي ستكون النتيجة وكأن نسبة الاشارة المستقبلة الى الضوضاء (SNR) اصبحت أعلى. تُظهر العديد من عمليات المحاكاة في هذا العمل أن مصفوفات SASPA قادرة على تقدير اتجاه الوصول بدقة أعلى بكثير من مصفوفات الهوائيات المتضمنة على هوائيات فعالة فقط، حتى عندما يكون حجم المصفوفة صغيرا ويكون استقبال الإشارات من اتجاهات حرجة ومتقاربة مكانيًا. تم فحص معيار الجذر التربيعي المتوسط للخطأ (RMSE) أيضًا، وقد وجد أن تقدير DoA باستخدام مجموعات SASPA يتطابق بشكل وثيق للغاية مع القيمة الحقيقية وعلى نطاق واسع من نسبة الإشارة إلى الضوضاء.

الكلمات الرئيسية – تحديد الاتجاه, خوارزمية ميوزك, مصفوفات هوائي فعال وهوائيات طفيلية متبادلة, معيار الجذر التربيعي المتوسط للخطأ.